Original scientific paper
https://doi.org/10.33180/InfMIDEM2023.403

Informacije MIDEM
Journal of Microelectronics, Electronic Components and Materials
Vol. 53, No. 4(2023), 233 – 238

Linear Thermal Expansion of $0.5Ba(Zr_{0.2}Ti_{0.8})O_3$-$0.5(Ba_{0.7}Ca_{0.3})TiO_3$ Bulk Ceramic

Sabi William Konsago[1,2], Andrej Debevec[1], Jena Cilenšek[1], Brigita Kmet[1,2], Barbara Malič[1,2]

[1]Electronic Ceramics Department, Jožef Stefan Institute, Ljubljana, Slovenia
[1]Jožef Stefan International Postgraduate School, Ljubljana, Slovenia

Abstract: We report the linear thermal expansion coefficient of lead-free ferroelectric ceramic barium zirconate titanate - barium calcium titanate $0.5Ba(Zr_{0.2}Ti_{0.8})O_3$-$0.5(Ba_{0.7}Ca_{0.3})TiO_3$ (BZT-BCT). The material was prepared by solid-state synthesis and consolidated by sintering at 1450°C. BZT-BCT crystallizes in the perovskite phase. The microstructure of the ceramic with about 95 % relative density consists of about 10 μm-sized grains. The contact dilatometry of the ceramic specimen reveals the change of slope of the linear thermal expansion curve at 84°C. This is in good agreement with the peak of the dielectric permittivity versus temperature at about 85°C indicating the transition from the low-temperature polar ferroelectric phase to a high-temperature nonpolar phase or Curie temperature. The thermal expansion coefficients of the polar tetragonal and nonpolar cubic phases of BZT-BCT are 7.69×10^{-6} K^{-1} (40°C – 80°C) and 12.39×10^{-6} K^{-1} (100°C – 600°C), respectively. The thermal expansion data are among the material data needed in the design of thin- and thick-film structures for energy-harvesting and energy-storage applications.

Keywords: $0.5Ba(Zr_{0.2}Ti_{0.8})O_3$-$0.5(Ba_{0.7}Ca_{0.3})TiO_3$ (BZT-BCT), lead-free, ferroelectric ceramic, linear thermal expansion

Linearni temperaturni raztezek volumenske keramike $0.5Ba(Zr_{0.2}Ti_{0.8})O_3$-$0.5(Ba_{0.7}Ca_{0.3})TiO_3$

Izvleček: V delu poročamo o linearnem temperaturnem raztezku volumenske keramike barijevega cirkonata titanata - barijevega kalcijevega titanata $0.5Ba(Zr_{0.2}Ti_{0.8})O_3$-$0.5(Ba_{0.7}Ca_{0.3})TiO_3$ (BZT-BCT). Material smo pripravili s sintezo v trdnem stanju in sintranjem pri 1450°C. BZT-BCT kristalizira v perovskitni fazi. Mikrostrukturo keramike s ≈95% relativno gostoto sestavljajo zrna velikosti okrog 10 μm. Linearni temperaturni raztezek keramike smo izmerili s kontaktno dilatometrijo od sobne temperature do 600°C. Pri temperaturi 84°C opazimo spremembo naklona krivulje raztezka. Ta podatek se ujema s temperaturo maksimuma dielektričnosti v odvisnosti od temperature, ki označuje prehod nizkotemperaturne polarne feroelektrične faze v visokotemperaturno nepolarno fazo oziroma Curiejevo temperaturo. Vrednosti linearnega temperaturnega raztezka polarne in nepolarne faze BZT-BCT sta 7.69×10^{-6} K^{-1} (40°C – 80°C) in 12.39×10^{-6} K^{-1} (100°C – 600°C). Podatke o temperaturnem raztezku keramike potrebujemo pri načrtovanju tanko- in debeloplastnih struktur, namenjenih zbiranju in shranjevanju energije.

Ključne besede: $0.5Ba(Zr_{0.2}Ti_{0.8})O_3$-$0.5(Ba_{0.7}Ca_{0.3})TiO_3$ (BZT-BCT), brez svinca, feroelektrična keramika, linearni temperaturni raztezek

** Corresponding Author's e-mail: barbara.malic@ijs.si*

1 Introduction

The discovery of the high piezoelectric properties of the barium zirconate titanate - barium calcium titanate solid solution $0.5Ba(Zr_{0.2}Ti_{0.8})O_3$-$0.5(Ba_{0.7}Ca_{0.3})TiO_3$ (BZT-BCT) bulk ceramic has revealed its great potential for many piezoelectric applications including actuators, transducers, and energy harvesting devices [1] - [3]. As an example, an intravascular ultrasound transducer made of BZT-BCT has been prototyped [4]. It is also being studied as a promising biocompatible material for bone regeneration [5], [6]. BZT-BCT has gained the attention of the ferroelectric/piezoelectric communities as one of the most promising environment-friendly alternatives to commercially widely spread lead-based piezoelectric ceramic materials such as $Pb(Zr,Ti)O_3$ (PZT) due to the Restriction of Hazardous Substances

How to cite:
S. W. Konsago et al., "Linear Thermal Expansion of $0.5Ba(Zr_{0.2}Ti_{0.8})O_3$-$0.5(Ba_{0.7}Ca_{0.3})TiO_3$ Bulk Ceramic", Inf. Midem-J. Microelectron. Electron. Compon. Mater., Vol. 53, No. 3(2023), pp. 233–238

(RoHS) regulations [7] - [9]. Recently it has been reported that it possesses promising energy storage properties [10], [11].

BZT-BCT exhibits a Curie temperature of about 85-90 °C. In the proximity of room temperature, the coexistence of rhombohedral, orthorhombic, and tetragonal phases of solid solutions of $Ba(Zr_{0.2}Ti_{0.8})O_3$ and $(Ba_{0.7}Ca_{0.3})TiO_3$ with the molar ratios close to unity contributes to enhanced piezoelectric properties [12], [13]. It was shown that the grain size strongly influences the piezoelectric properties and the phase transitional behaviour of BZT-BCT bulk ceramic; the enhanced piezoelectric response was characteristic for grain sizes exceeding 10 μm [14].

In numerous miniature devices, such as microelectromechanical systems (MEMS) or energy harvesters, the space constraints favour the use of piezoelectric ceramic elements in the form of thin or thick films [15], [16]. One of the key parameters for designing such devices includes the thermal expansion coefficients of the constituent materials. In case of a large difference in thermal expansion coefficients of the film and the substrate, the induced stresses may contribute to lowering the piezoelectric response [17] - [19]. Clamping the screen-printed thick film by the substrate results in poor densification during sintering [20]. Tensile stresses in the film that arise due to the thermal expansion coefficient mismatch may lead to the evolution of cracks [19]. Various effects of stresses generated by the thermal expansion mismatch also affect other functional properties, such as breakdown strength [21], [22], which is important in energy storage applications.

There are some publications on the thermal expansion coefficient of Ca- and Zr-modified barium titanate ceramics [23] - [26] but to our knowledge, there is no reported study on the linear thermal expansion coefficient of BZT-BCT ceramic. Such data would contribute to efficiently designing the processing of dense and crack-free BZT-BCT thick films where the powder slurry is screen-printed on a platinized alumina substrate. Such films could find applications in energy harvesting.

Our study aims to prepare perovskite BZT-BCT ceramic with a high relative density, uniform microstructure, and adequate low- and high-field dielectric properties. The linear thermal expansion coefficient from room temperature to 600 °C is measured.

2 Materials and methods

BZT-BCT powder was prepared using alkaline earth carbonates ($BaCO_3$, 99.8% and $CaCO_3$, 99,95% both from Alfa Aesar, Karlsruhe, Germany) and transition metal oxides (TiO_2, 99.8% also from Alfa Aesar, Karlsruhe, Germany and ZrO_2, 99.8% from Tosoh, Japan). The metal content was checked gravimetrically. The 25 g batches of stoichiometric fractions of the reagents were homogenized using isopropanol in a planetary mill (PM 400, Retsch) with yttria-stabilized zirconia milling bodies (3 mm, Tosoh, Japan) for 2 h at 200 rpm. The median particle size of the milled powder was 0.45 μm as determined by laser granulometry (Microtrac S3500 Particle Size Analyzer) using isopropanol as a dispersion liquid. The calcination of the loosely pressed reagent mixture (P = 50 MPa) took place at 1300 °C for 4 hours in the air with heating and cooling rates of 5 K/min. The powder was again milled for 2h at 200 rpm in a planetary mill, dried at 120 °C and sieved. The powder was shaped into pellets (diameter: 8 mm) or bars (40 mm x ≈7 mm x ≈5 mm) by uniaxial (P = 50 MPa) and isostatic pressing (P = 300 MPa). The powder compacts were sintered at 1450 °C for 4 hours in the air with heating and cooling rates of 5 K/min.

The phase composition of the calcined powders and crushed sintered specimens was analyzed by X-ray diffraction (XRD, X'Pert PRO MPD, PANanalytical, CuKa1 radiation, time/step: 100 s, interval between data points: 0.0016°). The density of the sintered samples was determined pycnometrically (Micromeritics, AccuPyc III 1340 Pycnometer).

The ceramic samples were ground and polished using standard ceramographic techniques. Thermal etching of the polished sections at 1350 °C for a few minutes revealed the grain boundaries. A field-emission scanning electron microscope (FE-SEM JEOL JSM-7600) with an energy-dispersive X-ray spectrometer (EDXS, INCA Oxford 350 EDS SDD) was used for the analysis of the microstructure. The grain size was determined using the Image Tool software.

For low- and high-field dielectric measurements, the disks were cut to the thickness of 0.5 mm and polished. An annealing step to 600 °C for 1 h followed by a slow cooling (1 K/min) was used to release the stresses of mechanical operations. The Au electrodes with a diameter of 3 mm were RF-magnetron sputtered on the faces of the disks (5 Pascal). The dielectric permittivity (ε) and losses ($\tan\delta$) were measured between +150 °C and -40°C with a cooling rate of 1 K/min (Agilent E4980A Precision LCR meter, 1V). The polarization-electric field hysteresis loops were measured at room temperature with a sine voltage at the frequency of 50 Hz (Aixacct TF analyzer 2000).

For the measurement of the thermal expansion, the ceramic bars were cut to the dimensions of 25 mm x 5 mm x 4 mm. The faces of the bars were plan-parallel

polished. Thermal stresses were released as described above. The dimensional changes of the specimen upon heating and cooling were measured with a contact dilatometer with a corundum measuring system (Netzsch DIL 402 PC) between room temperature and 600 °C with the heating and cooling rates of 5 K/min in air.

3 Results and discussion

Figure 1 contains the XRD patterns of BZT-BCT powder after the calcination at 1300 °C (a) and the ceramic sintered at 1450 °C (b). The XRD patterns of both samples reveal a perovskite phase without any noticeable secondary phases. The unit cell distortion could not be determined using a standard X-ray diffractometer, synchrotron radiation would be needed to obtain a deeper insight into the phase composition of the material, c.f. [13], [27] - [29]. According to the phase diagram [13], the coexistence of the orthorhombic phase cannot be excluded at room temperature besides rhombohedral and tetragonal phases in the morphotropic phase boundary region.

The relative density of BZT-BCT ceramic is 95.4 %. The microstructure shown in Figure 2 a) is uniform, with a unimodal grain size distribution and a mean grain size of 9.66 ± 4.84 μm (Figure 2 b)). EDXS analysis confirmed a uniform distribution of elements within and between individual grains (EDXS spectra are not shown). Trace amounts of a secondary phase were observed at some grain junctions (see the inset of Figure 2 a)) but due to their small size, their chemical composition could not be reliably determined on the level of FE-SEM.

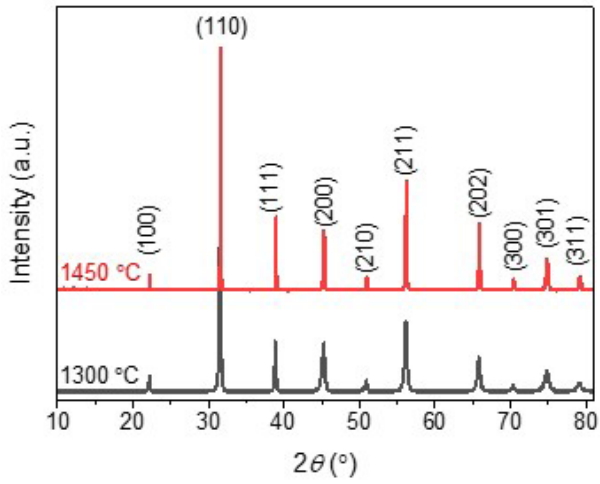

Figure 1: XRD patterns of BZT-BCT powder calcined at 1300 °C and ceramic sintered at 1450 °C. The peaks are indexed according to the $BaTiO_3$ cubic phase (PDF 01-074-4539).

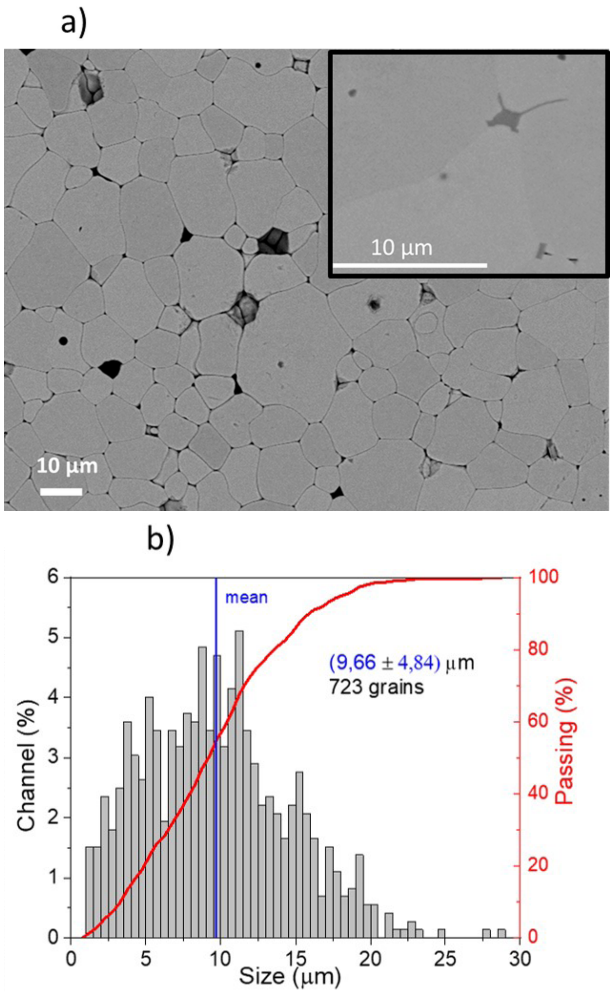

Figure 2: a) SEM micrograph of the microstructure of BZT-BCT ceramic and b) grain size distribution. Inset in panel a) reveals an intergranular phase located at a grain junction.

Figure 3 shows the temperature dependence of the dielectric permittivity and losses as a function of temperature in the frequency range from 100 Hz to 100 kHz. Dielectric permittivity and losses at room temperature and 1 kHz are 3165 and 0.029 in agreement with reported values for ceramics with similar grain sizes [14]. There is no significant change in the dielectric permittivity in the frequency range from 100 Hz to 100 kHz in the measured temperature range. The change of slope at about 40 °C is attributed to the rhombohedral–tetragonal phase transition, and the dielectric permittivity peak at about 85 °C to transition to the cubic phase or Curie temperature. The grain size influences both phase transition temperatures; for the ceramic with about 10 μm-sized grains, the respective values were 87 °C and 35 °C [14]. Broadening of the permittivity peak, characteristic of polycrystalline ferroelectrics, is related to the micron size of the crystallites and the presence of two cations on each cation sublattice

site. We do not observe any noticeable frequency peak shifting in the measured frequency range supporting the ferroelectric nature of the BZT-BCT ceramic. It has been shown that processing conditions and grain size strongly influence the ferroelectric or relaxor nature of BZT-BCT [14], [27].

Figure 4 shows the room temperature polarization–electric field (*P–E*) hysteresis loops measured at 50 Hz. The sample survived the maximum applied field of 70 kV/cm, indicating its good dielectric breakdown resistance. The remnant polarization P_r and coercive field E_c are about 13 μC/cm^2 and 5.9 kV/cm, respectively, indicating a good ferroelectric response of BZT-BCT. Hao et al obtained similar P_r and E_c values for the ceramic with 10 μm-sized grains [14].

Figure 5 shows the dilatometric curves of BZT-BCT ceramic, revealing linear thermal expansion or contraction upon heating or cooling. There is not much difference between the heating and cooling curves. Two main slopes are discerned in both cases with the inflexion point at 84.0 °C. The thermal hysteresis between the heating and cooling runs is quite small. We note that the inflexion temperature corresponds well to the dielectric permittivity peak temperature, cf. Figure 3. The thermal expansion coefficient (TEC = $(\Delta L/L_0)/\Delta T$), determined from the cooling curve in the temperature range from 40 °C to 80 °C, is 7.69×10^{-6} K^{-1}. In this temperature range the tetragonal phase prevails [13], but the coexistence of a rhombohedral phase cannot be excluded judging from the evident change of slope at about 40 °C in the dielectric permittivity curve (cf. Figure 3). As the temperature increases, the TEC progressively increases as well. From 100 °C to the final temperature of 600 °C, in the temperature range of the cubic phase, the TEC is 12.39×10^{-6} K^{-1}.

As explained earlier we could not find the thermal expansion data for BZT-BCT. The TEC of the base formulation of BZT-BCT solid solution, the prototype ferroelectric $BaTiO_3$, is 6.5×10^{-6} K^{-1} in the tetragonal phase and 9.8×10^{-6} K^{-1} in the cubic phase (125 °C – 200 °C) measured by contact dilatometry [30]. It is noted that the change in the slope of the thermal expansion of $BaTiO_3$ at the phase transition temperature is sharp and accompanied by a noticeable shrinkage which is a fingerprint of a first-order phase transition and is not the case with BZT-BCT. Here, we observe only the change in the slope of the thermal expansion. Tian et al. studied $(Ba,Ca)TiO_3$-$Ba(Zr,Ti)O_3$ with slightly different molar ratios of cations compared to BZT-BCT formulation, and they incorporated various rare-earth dopants. They measured a TEC of about 5×10^{-6} K^{-1} at lower temperatures and a TEC of about 11×10^{-6} K^{-1} at higher temperatures, the final temperature being 400 °C. The exact value of TEC and the TEC-inflexion point's temperature depended on the studied materials' chemical composition[31], [32]. Our results are in good agreement with these latter dilatometric studies of the $(Ba,Ca)TiO_3$-$Ba(Zr,Ti)O_3$ solid solutions.

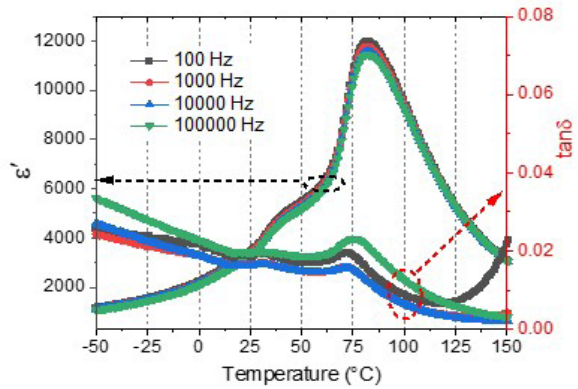

Figure 3: The dielectric permittivity and losses as a function of the temperature of BZT-BCT ceramic.

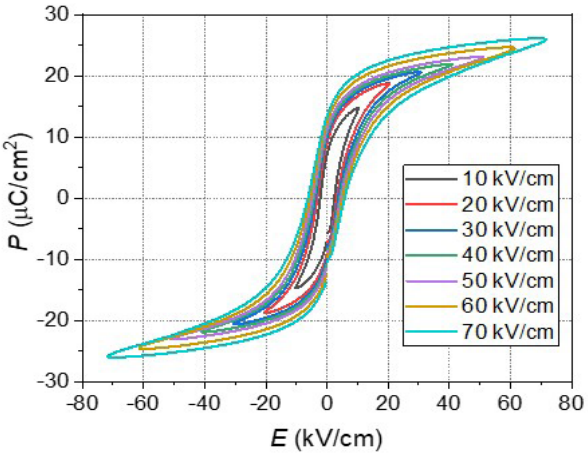

Figure 4: Polarization - electric field- loops of BZT-BCT ceramic measured at 50 Hz and room temperature.

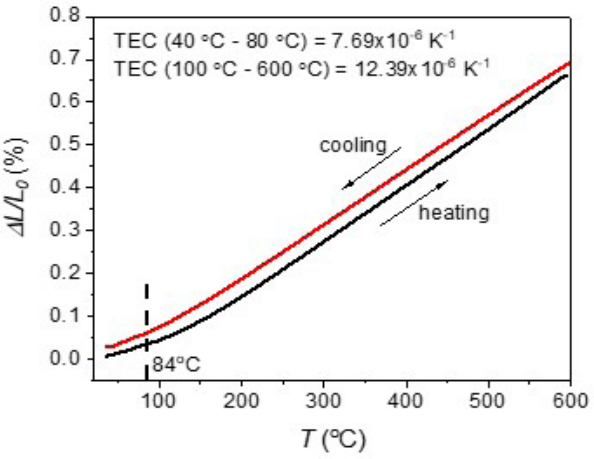

Figure 5: The linear thermal expansion of BZT-BCT ceramic measured between room temperature and 600 °C. The inflexion point and TEC were determined from the cooling curve.

4 Conclusions

In conclusion, this study focused on determining the thermal expansion behavior of $0.5Ba(Zr_{0.2}Ti_{0.8})O_3$-$05(Ba_{0.7}Ca_{0.3})TiO_3$ (BZT-BCT) bulk ceramic. The powder, prepared by solid-state synthesis, was compacted and sintered to a high relative density at 1450 °C for 4 hours. The ceramic crystallized in the perovskite phase. The microstructure consisted of about 10 μm sized grains. The measurement of the dielectric permittivity versus temperature revealed two anomalies which could be related to the phase transitions of the predominantly rhombohedral to tetragonal phase at about 40 °C and to cubic phase at about 90 °C. The hysteretic dependence of the polarization versus the electric field confirmed the ferroelectric nature of the ceramic. The dilatometric measurements revealed the thermal expansion coefficients of the polar and cubic phases of 7.69×10^{-6} K^{-1} (40 °C – 80 °C) and 12.39×10^{-6} K^{-1} (100 °C – 600 °C). The study results contribute to the design of thick and thin-film structures based on BZT-BCT in various energy-harvesting and/or energy-storage applications.

5 Acknowledgments

The authors acknowledge the advice and technical support of Silvo Drnovšek, Electronic Ceramics Department, Jožef Stefan Institute.

6 Conflict of interest

The authors declare no conflict of interest.

The authors acknowledge the financial support of the Slovenian Research Agency (core funding P2-0105).

7 References

1. W. Liu and X. Ren, "Large piezoelectric effect in Pb-free ceramics," *Phys Rev Lett*, vol. 103, no. 25, 257602, Dec. 2009, https://doi.org/10.1103/PhysRevLett.103.257602.
2. M. Acosta, N. Novak, W. Jo, and J. Rödel, "Relationship between electromechanical properties and phase diagram in the $Ba(Zr_{0.2}Ti_{0.8})O_3$-x $(Ba_{0.7}Ca_{0.3})TiO_3$ lead-free piezoceramic," *Acta Mater*, vol. 80, pp. 48–55, 2014, https://doi.org/10.1016/j.actamat.2014.07.058.
3. J. Rödel, K. G. Webber, R. Dittmer, W. Jo, M. Kimura, and D. Damjanovic, "Transferring lead-free piezoelectric ceramics into application," *J Eur Ceram Soc*, vol. 35, no. 6, pp. 1659–1681, Jun. 2015, https://doi.org/10.1016/j.jeurceramsoc.2014.12.013.
4. X. Yan *et al.*, "Correspondence: Lead-free intravascular ultrasound transducer using BZT-50BCT ceramics," *IEEE Trans Ultrason Ferroelectr Freq Control*, vol. 60, no. 6, pp. 1272–1276, 2013, https://doi.org/10.1109/TUFFC.2013.2692.
5. K. K. Poon, M. C. Wurm, D. M. Evans, M. Einarsrud, R. Lutz, and J. Glaum, "Biocompatibility of (Ba,Ca)$(Zr,Ti)O_3$ piezoelectric ceramics for bone replacement materials," *J Biomed Mater Res B Appl Biomater*, vol. 108, no. 4, pp. 1295–1303, May 2020, https://doi.org/10.1002/jbm.b.34477.
6. C. S. Manohar *et al.*, "Novel Lead-free biocompatible piezoelectric Hydroxyapatite (HA) – BCZT $(Ba_{0.85}Ca_{0.15}Zr_{0.1}Ti_{0.9}O_3)$ nanocrystal composites for bone regeneration," *Nanotechnol Rev*, vol. 8, no. 1, pp. 61–78, May 2019, https://doi.org/10.1515/ntrev-2019-0006.
7. "DIRECTIVE 2002/95/EC OF THE EUROPEAN PARLIAMENT AND OF THE COUNCIL of 27 January 2003 on the restriction of the use of certain hazardous substances in electrical and electronic equipment."
8. "JIS-C-0950: 2005 (E), 'The marking for presence of the specific chemical substances for electrical and electronic equipment', Japanese Standards Association, 2005".
9. L. M. Benson and K. K. Reczek, "A guide to United States electrical and electronic equipment compliance requirements," Jun. 2021. https://doi.org/10.6028/NIST.IR.8118r2.
10. V. S. Puli *et al.*, "Structure, dielectric, ferroelectric, and energy density properties of (1 – x)BZT–xBCT ceramic capacitors for energy storage applications," *J Mater Sci*, vol. 48, no. 5, pp. 2151–2157, Mar. 2013, https://doi.org/10.1007/s10853-012-6990-1.
11. Neha, R. Pandey, M. Bhatnagar, P. Kumar, R. K. Malik, and C. Prakash, "Improved dielectric and energy storage properties in $(1\text{-}x)BaTi_{0.80}Zr_{0.20}O_3$-$xBa_{0.70}Ca_{0.30}Ti_{0.99}Fe_{0.01}O_3$ ceramics near morphotropic phase boundary," *Mater Lett*, vol. 318, 132126, Jul. 2022, https://doi.org/10.1016/j.matlet.2022.132126.
12. M. Acosta, N. Novak, G. A. Rossetti, and J. Rödel, "Mechanisms of electromechanical response in (1 - X)$Ba(Zr_{0.2}Ti_{0.8})O_3$-x$(Ba_{0.7}Ca_{0.3})TiO_3$ ceramics," *Appl Phys Lett*, vol. 107, no. 14, 142906, Oct. 2015, https://doi.org/10.1063/1.4932654.
13. D. S. Keeble, F. Benabdallah, P. A. Thomas, M. Maglione, and J. Kreisel, "Revised structural phase diagram of $(Ba_{0.7}Ca_{0.3}TiO_3)$-$(BaZr_{0.2}Ti_{0.8}O_3)$," *Appl Phys Lett*, vol. 102, no. 9, 092903, Mar. 2013, https://doi.org/10.1063/1.4793400.

14. J. Hao, W. Bai, W. Li, and J. Zhai, "Correlation between the microstructure and electrical properties in high-performance $(Ba_{0.85}Ca_{0.15})(Zr_{0.1}Ti_{0.9})O_3$ lead-free piezoelectric ceramics," *Journal of the American Ceramic Society*, vol. 95, no. 6, pp. 1998–2006, Jun. 2012, https://doi.org/10.1111/j.1551-2916.2012.05146.x.
15. L. Song, S. Glinsek, S. Drnovsek, V. Kovacova, B. Malic, and E. Defay, "Piezoelectric thick film for power-efficient haptic actuator," *Appl Phys Lett*, vol. 121, no. 21, 212901, Nov. 2022, https://doi.org/10.1063/5.0106174.
16. P. Muralt, "Polar oxide thin films for MEMS applications," T. Schneller, R. Waser, M. Kosec and D. Payne (Eds.), *Chemical Solution Deposition of Functional Oxide Thin Films, Wien, Austria, Springer-Verlag, 2013, Ch. 24, pp. 593-620*. https://doi.org/10.1007/978-3-211-99311-8_24.
17. T. A. Berfield, R. J. Ong, D. A. Payne, and N. R. Sottos, "Residual stress effects on piezoelectric response of sol-gel derived lead zirconate titanate thin films," *J Appl Phys*, vol. 101, no. 2, 024102, Jan. 2007, https://doi.org/10.1063/1.2422778.
18. L. Lian and N. R. Sottos, "Effects of thickness on the piezoelectric and dielectric properties of lead zirconate titanate thin films," *J Appl Phys*, vol. 87, no. 8, pp. 3941–3949, Apr. 2000, https://doi.org/10.1063/1.372439.
19. K. Coleman, J. Walker, T. Beechem, and S. Trolier-McKinstry, "Effect of stresses on the dielectric and piezoelectric properties of $Pb(Zr_{0.52}Ti_{0.48})O_3$ thin films," *J Appl Phys*, vol. 126, no. 3, 034101, Jul. 2019, https://doi.org/10.1063/1.5095765.
20. R. K. BORDIA and R. RAJ, "Sintering Behavior of Ceramic Films Constrained by a Rigid Substrate," *Journal of the American Ceramic Society*, vol. 68, no. 6, pp. 287–292, Jun. 1985, https://doi.org/10.1111/j.1151-2916.1985.tb15227.x.
21. A. M. Pashaev, A. Kh. Dzhanakhmedov, and A. A. Aliyev, "Effect of Tensile Stresses on the Breakdown Voltage of Thin Films," *Technical Physics*, vol. 65, no. 1, pp. 54–56, Jan. 2020, https://doi.org/10.1134/S1063784220010211.
22. Y.-N. Bie *et al.*, "Effect of Source Field Plate Cracks on the Electrical Performance of AlGaN/GaN HEMT Devices," *Crystals (Basel)*, vol. 12, no. 9, 1195, Aug. 2022, https://doi.org/10.3390/cryst12091195.
23. Y. Tian *et al.*, "Diversiform electrical and thermal expansion properties of $(1-x)Ba_{0.95}Ca_{0.05}Ti_{0.94}Zr_{0.06}O_3$–(x)Dy lead-free piezoelectric ceramics influenced by defect complexes," *J Mater Sci*, vol. 53, no. 16, pp. 11228–11241, Aug. 2018, https://doi.org/10.1007/s10853-018-2428-8.
24. Y. Tian *et al.*, "Electrical Properties and Thermal Expansion Characteristics of $(1-x)Ba_{0.948}Ca_{0.05}Er_{0.002}Ti_{0.94}Zr_{0.06}O_3$–(x)Pr Lead-Free Piezoelectric Ceramics Sintered at a Low-Temperature," *physica status solidi (a)*, vol. 216, no. 2, 1800622, Jan. 2019, https://doi.org/10.1002/pssa.201800622.
25. Y. Tian *et al.*, "Temperature-dependent ferroelectric and piezoelectric response of Yb^{3+} and Tm3+ co-doped $Ba_{0.95}Ca_{0.05}Ti_{0.90}Zr_{0.10}O_3$ lead-free ceramic," *Journal of Ceramic Processing Research*, vol. 23, no. 4, pp. 430–435, Aug. 2022, https://doi.org/10.36410/jcpr.2022.23.4.430.
26. Y. Tian *et al.*, "Piezoelectricity and Thermophysical Properties of $Ba_{0.90}Ca_{0.10}Ti_{0.96}Zr_{0.04}O_3$ Ceramics Modified with Amphoteric Nd3+ and Y3+ Dopants," *Materials*, vol. 16, no. 6, 2369, Mar. 2023, https://doi.org/10.3390/ma16062369.
27. F. Benabdallah *et al.*, "Structure–microstructure–property relationships in lead-free BCTZ piezoceramics processed by conventional sintering and spark plasma sintering," *J Eur Ceram Soc*, vol. 35, no. 15, pp. 4153–4161, Dec. 2015, https://doi.org/10.1016/j.jeurceramsoc.2015.06.030.
28. H. Amorín *et al.*, "Insights into the Early Size Effects of Lead-Free Piezoelectric $Ba_{0.85}Ca_{0.15}Zr_{0.1}Ti_{0.9}O_3$," *Adv Electron Mater*, https://doi.org/10.1002/aelm.202300556.
29. S. López-Blanco, D. A. Ochoa, H. Amorín, A. Castro, M. Algueró, and J. E. García, "Fine-grained high-performance $Ba_{0.85}Ca_{0.15}Zr_{0.1}Ti_{0.9}O_3$ piezoceramics obtained by current-controlled flash sintering of nanopowders," *J Eur Ceram Soc*, vol. 43, no. 16, pp. 7440–7445, Dec. 2023, https://doi.org/10.1016/j.jeurceramsoc.2023.08.012.
30. G. Shirane and A. Takeda, "Volume Change at Three Transitions in $BaTiO_3$ Ceramics," *J Physical Soc Japan*, vol. 6, no. 2, pp. 128–129, Mar. 1951, https://doi.org/10.1143/JPSJ.6.128.
31. Y. Tian *et al.*, "Diversiform electrical and thermal expansion properties of $(1-x)Ba_{0.95}Ca_{0.05}Ti_{0.94}Zr_{0.06}O_3$–(x)Dy lead-free piezoelectric ceramics influenced by defect complexes," *J Mater Sci*, vol. 53, no. 16, pp. 11228–11241, Aug. 2018, https://doi.org/10.1007/s10853-018-2428-8.
32. Y. Tian *et al.*, "Temperature-dependent ferroelectric and piezoelectric response of Yb^{3+} and Tm^{3+} co-doped $Ba_{0.95}Ca_{0.05}Ti_{0.90}Zr_{0.10}O_3$ lead-free ceramic," *Journal of Ceramic Processing Research*, vol. 23, no. 4, pp. 430–435, Aug. 2022, https://doi.org/10.36410/jcpr.2022.23.4.430.

Arrived: 09. 01. 2024
Accepted: 13. 02. 2024